Water-Driven Micromotors for Rapid Photocatalytic Degradation of Biological and Chemical Warfare Agents

Jinxing Li, Virendra V. Singh, Sirilak Sattayasamitsathit, Jahir Orozco, Kevin Kaufmann, Renfeng Dong, Wei Gao, Beatriz Jurado-Sanchez, Yuri Fedorak, and Joseph Wang*

Department of Nanoengineering, University of California, San Diego, La Jolla, California 92093, United States

ABSTRACT Threats of chemical and biological warfare agents (CBWA) represent a serious global concern and require rapid and efficient neutralization methods. We present a highly effective micromotor strategy for photocatalytic degradation of CBWA based on light-activated TiO_2/Au/Mg microspheres that propel autonomously in natural water and obviate the need for external fuel, decontaminating reagent, or mechanical agitation. The activated TiO_2/Au/Mg micromotors generate highly reactive oxygen species responsible for the efficient destruction of the cell membranes of the anthrax simulant *Bacillus globigii* spore, as well as rapid and complete *in situ* mineralization of the highly persistent organophosphate nerve agents into nonharmful products. The water-driven propulsion of the TiO_2/Au/Mg micromotors facilitates efficient fluid transport and dispersion of the photogenerated reactive oxidative species and their interaction with the CBWA. Coupling of the photocatalytic surface of the micromotors and their autonomous water-driven propulsion thus leads to a reagent-free operation which holds a considerable promise for diverse "green" defense and environmental applications.

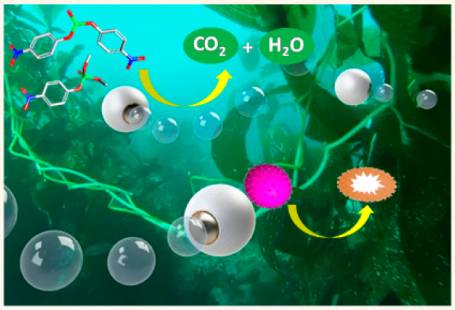

KEYWORDS: micromotors · biological agents · chemical warfare defense · photocatalytic degradation · titanium dioxide

Concerns over chemical and biological warfare agents (CBWA), such as *Bacillus anthracis* and nerve agents, have increased greatly over the past decades.[1] Spores of *Bacillus anthracis*, the bacterium that causes anthrax, have emerged as one of the most dangerous biological agents because they are dormant, tough, and temporarily nonreproductive structures that can survive over extended periods without nutrients.[2] Similarly, nerve agents are considered the most nefarious synthetic chemical compounds that threaten humans and the environment because of their phosphorylating mode of action.[3]

One of the most promising approaches for CBWA degradation is photocatalytic degradation by titanium dioxide (TiO_2).[4−6] The photocatalytic decontamination processes of TiO_2 do not require harsh reagents or yield toxic byproducts, making it one of the most efficient and environmentally friendly materials for the degradation of contaminants.[4−6] TiO_2 also exerts antispore activity against a variety of *Bacillus* species.[7] However, the photocatalytic oxidation over the TiO_2 surface can be hindered by the accumulation of intermediate species on the catalyst surface.[8] In addition, eliminating stockpiles of CBWA in remote storage locations commonly requires controlled agitation (mixing) of the contaminated solution which is challenging for practical field detoxification applications of TiO_2.

We report here on a new powerful micromotor strategy for the rapid photocatalytic destruction of CBWA. The recent development of artificial nano/micromotors has paved the way to major advances in nanoscience.[9−20] Operating on locally supplied fuels, such as hydrogen peroxide, these self-propelled motors have demonstrated a wide range of practical applications, ranging from cancer cell isolation to the delivery of therapeutic payloads.[21−28] Autonomously moving chemically powered micromotors have been shown recently to be extremely useful for enhancing the degradation of chemical

* Address correspondence to josephwang@ucsd.edu.

Received for review September 5, 2014 and accepted October 7, 2014.

Published online October 07, 2014
10.1021/nn505029k

pollutants.[29−34] However, such motor-based remediation protocols commonly require the addition of external peroxide fuel and of decontaminating reagents and often lead to incomplete pollutant degradation, hence hindering practical *in situ* environmental and defense applications. In addition, the ability of motor-based remediation protocols to degrade biological agents has not been demonstrated.

In the following sections, we will illustrate that magnesium-based spherical micromotors, coated with a highly photoactive titanium dioxide film (containing gold nanoparticles), can be self-propelled in natural water environments to offer a highly efficient photocatalytic decomposition of biological and chemical warfare agents (Figure 1). In contrast to existing peroxide-driven microrockets for pollutant degradation,[29,30] the new water-driven TiO_2/Au/Mg micromotors offer complete and rapid oxidative degradation of CBWA without adding an external peroxide fuel or a decontaminating reagent. Owing to its extremely attractive performance and distinct advantages, the new "on-the-fly" photocatalytic concept could have broad implications upon the efficiency and speed of a wide range of defense and environmental neutralization processes.

RESULTS AND DISCUSSION

As illustrated schematically in Figure 1, to achieve such environmentally friendly effective CBWA degradation, we combined the photocatalytic activity of TiO_2 with the water-powered propulsion of magnesium-based Janus microspheres. Such autonomous movement in natural environments reflects the hydrogen bubble thrust generated from the Mg−water reaction.[34,35] The new TiO_2/Au/Mg microsphere motors are composed of Mg microparticles coated nearly completely with a TiO_2 shell. These motors generate highly oxidative species (such as superoxide anions, peroxide radicals, hydroxyl radicals, and hydroxyl anions) on their UV-activated TiO_2 surface during their autonomous propulsion. The latter produces significant mixing during the photocatalytic decontamination process (without external forced convection) and leads to a remarkably effective photocatalytic cleaning microsystem. Of particular significance, the new TiO_2/Au/Mg micromotors display a remarkable antispore activity, as illustrated for the rapid inactivation of *Bacillus globigii* spores, a surrogate species of the biological warfare agent *Bacillus anthracis* spores. Dramatically improved decontamination efficiency and speed are also demonstrated for the fast *in situ* mineralization of the highly persistent organophosphate nerve agents, bis(4-nitrophenyl)phosphate (b-NPP) and methyl paraoxon (MP), into completely nonharmful products.

Figure 2A displays a diagram of the water-driven TiO_2/Au/Mg micromotors. The new micromotor design and composition allow replacement of the common, yet undesirable, hydrogen peroxide fuel of previous

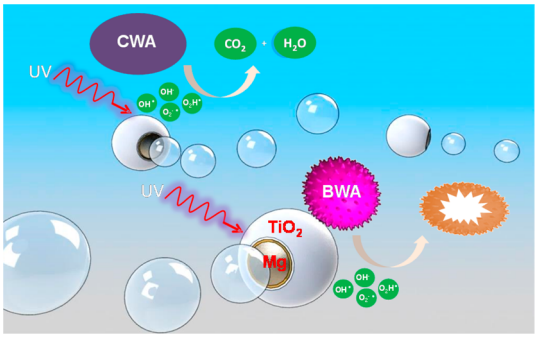

Figure 1. Schematic representation of the self-propulsion and photocatalytic degradation of biological warfare agents (BWA) and chemical warfare agents (CWA) into environmentally friendly products by water-driven spherical TiO_2/Au/Mg micromotors.

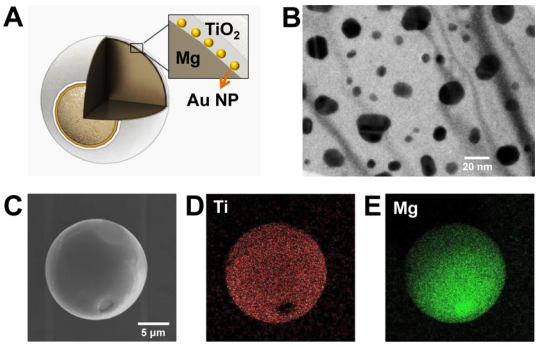

Figure 2. (A) Schematic image of a photoactive TiO_2/Au/Mg motor showing the Mg core, Au nanoparticles (Au NP) and TiO_2 shell layer. (B) Transmission electron microscopy image of Au nanoparticles embedded in the surface of TiO_2. (C) Scanning electron microscopy image of TiO_2/Au/Mg motor. (D,E) Energy-dispersive X-ray spectroscopy images illustrating the distribution of the titanium shell and the magnesium inner core, respectively.

chemically powered remediation micromotors with the aquatic media itself as an *in situ* fuel. The new motors were fabricated by dispersing Mg particles (average size of ~20 μm) on a glass slide and coating them first with a thin layer of Au nanoparticles by an altered sputtering process (see details in the Methods section). With the enhanced macrogalvanic corrosion by the Au nanoparticles and the pitting corrosion by the chloride ions, Mg can continuously reduce water to generate the hydrogen bubbles' thrust for a "green" propulsion process in chloride-rich natural environments.[34] Atomic layer deposition (ALD) has been used subsequently to grow the outer photoactive TiO_2 layer due to the remarkably conformal coating behavior of the process. Since such an ALD process utilizes gas phase reactants, it leads to uniform coatings over the Au-sputtered Mg microspheres, while still leaving a small opening at the contact point of the sphere to the glass slide. Transmission electron microscopy (TEM) was carried out to examine the size and morphology of the Au nanoparticles embedded in the TiO_2 shell, as displayed in the image of Figure 2B. It is observed that the size of Au nanoparticles is distributed

from 3 to 30 nm, which is crucial to increase the photooxidation efficiency of TiO_2 by shifting its Fermi level and enhancing the charge carrier separation.[36] The scanning electron microscopy (SEM) image of Figure 2C displays the morphology of a prepared TiO_2/Au/Mg micromotor, with a TiO_2 outer layer containing a small (~2 μm) opening that exposes the Mg core to the water fuel and facilitates directional H_2 bubble thrust. The presence of the TiO_2 coating, with a small spherical opening, is also confirmed by the corresponding energy-dispersive X-ray spectroscopy (EDX) mapping of Ti and Mg displayed in Figure 2D,E.

The new TiO_2/Au/Mg micromotors can operate in real-life aqueous environmental matrices containing chloride and surfactant, without adding external fuel to the sample matrix. As illustrated in Figure 3A, once the TiO_2/Au/Mg micromotors are immersed into chloride-rich environments (such as seawater), a spontaneous redox reaction—involving the oxidation of the Mg surface to reduce water for generation of hydrogen bubbles—takes place. The hydrogen bubbles, ejected from the exposed Mg "opening" of the microsphere, propel the micromotor in the opposite direction. The small opening enables a controlled reaction process and gradual dissolution of the Mg core, leading to a prolonged motor lifetime of approximately 15 min in connection to 20 μm spheres. Longer lifetimes can be obtained by using larger microspheres. The changes in the morphology of the micromotor before and after the propulsion process are clearly indicated by comparing the SEM images of Figure 3B (before immersion in the water media) and Figure 3C (after complete Mg dissolution). Continuous motion eventually leads to an empty TiO_2 microshell. Figure 3D,E, along with the corresponding Supporting Information video S1, illustrates the propulsion behavior of the micromotors in a 0.08 M NaCl solution, initially (D) and after 15 min propulsion (E). The tracking trajectories in Figure 3D,E display the motion over a 3 s period, with an average speed of ~80 μm/s, which corresponds to a relative speed of nearly four body lengths/s. Figure 3F and the corresponding Supporting Information video S2 illustrate the efficient movement of TiO_2/Au/Mg micromotors in a seawater sample. The track line over this 3 s period corresponds to a high speed of 110 μm/s. The increased speed of the micromotors in this natural water medium, compared to the 0.08 M NaCl aquatic medium, reflects the higher chloride concentration of seawater (~0.54 M NaCl) that accelerates the Mg erosion and the H_2 bubble evolution.[34,37] Supporting Information video S3 demonstrates that TiO_2/Au/Mg micromotors with a size of ~30 μm can lead to an efficient propulsion for 15 min in seawater. The attractive behavior of the TiO_2/Au/Mg micromotors in the chloride-rich medium indicates their promise for real-world environmental remediation (*e.g.*, decontamination of seawater).

The decontamination ability of the UV-irradiated TiO_2/Au/Mg micromotors associated with their continuous

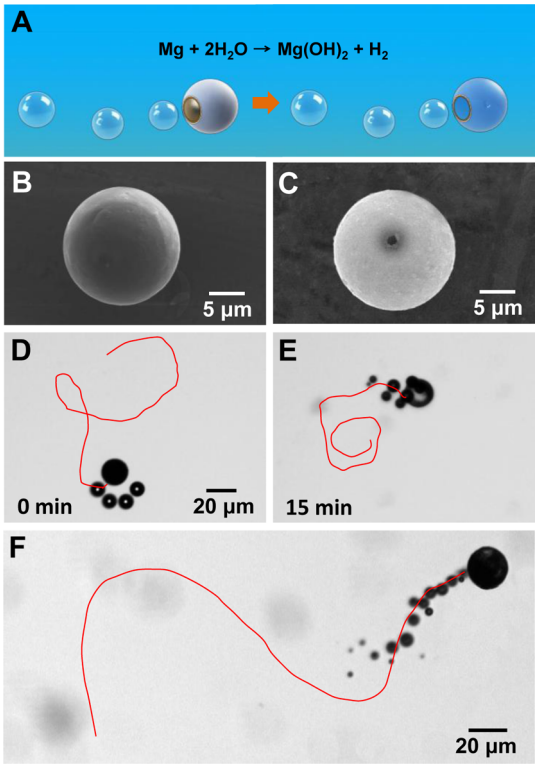

Figure 3. Propulsion of the TiO_2/Au/Mg micromotors. (A) Schematic of the propulsion process of the TiO_2/Au/Mg micromotor. (B) SEM image of a TiO_2/Au/Mg micromotor. (C) SEM images showing the morphology of a hollow TiO_2 shell resulting from the complete dissolution of the Mg core following 18 min movement of the motor. (D) Tracking lines (taken from Supporting Information video S1) illustrating the typical trajectories traveled by a TiO_2/Au/Mg micromotor in a 0.08 M NaCl solution over a 3 s interval at (D) t = 0 min and (E) t = 15 min. (F) Tracking line image illustrating the motors' propulsion over a 3 s period in 90% seawater (taken from Supporting Information video S2). Surfactant level (D−F), 0.075% Triton X-100.

motion has been investigated first by the photocatalytic degradation of nerve agent simulants, methyl paraoxon (MP) and bis(4-nitrophenyl)phosphate (b-NPP). The number of micromotors and the remediation time were optimized by using MP as a model agent. The micromotors were propelled in the contaminated solution (600 μL) in the presence of 0.08 M NaCl under UV light. The degradation percentage was calculated by the UV−vis absorbance spectra obtained during MP photodecomposition, characterized by the absorbance peak at 400 nm. It is observed the MP content decreased under irradiation with increased remediation time and motor numbers. A highly efficient MP degradation, corresponding to ~95% degradation, can be achieved by varying the number of TiO_2/Au/Mg micromotors to 3.08×10^5 (corresponding to 2.25 mg) and the UV remediation time to 10 min. These optimization studies indicate that small amounts of micromotors can lead to a near complete degradation of chemical warfare agents within very short time periods, indicating considerable promise for large-scale degradation of toxic agents.

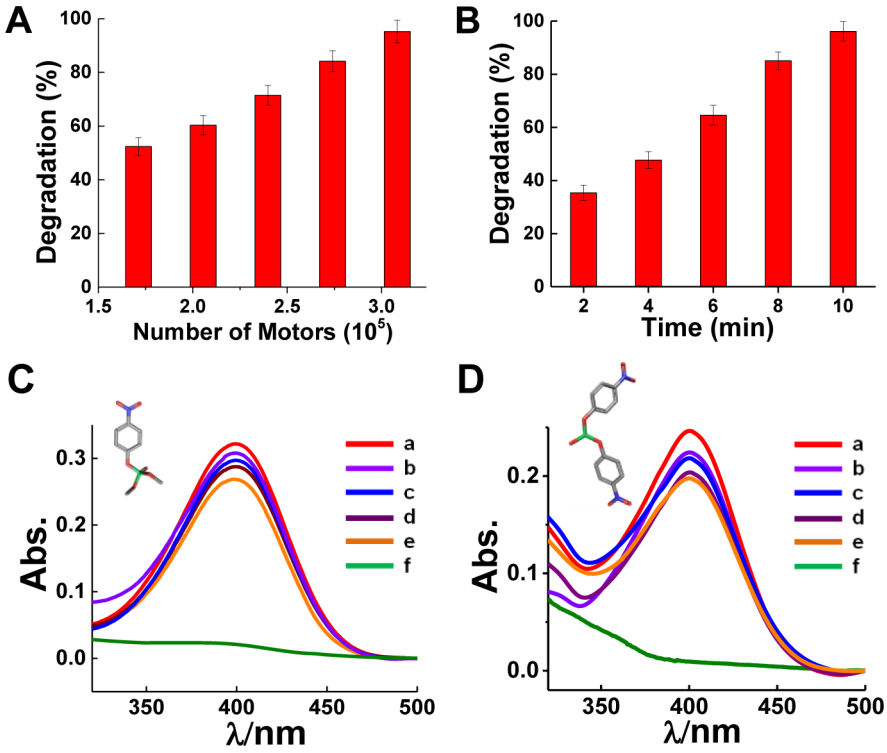

Figure 4. "On-the-fly" photocatalytic degradation of chemical warfare agents using TiO_2/Au/Mg micromotors. Effect of the (A) number of micromotors and (B) remediation time on the photodegradation efficiency of MP. The amount of the TiO_2/Au/Mg micromotors was varied from 1.71×10^5 to 3.08×10^5, while the remediation time was varied from 0 to 10 min. Absorbance spectra of the 1.7 μM (C) MP and (D) b-NPP, after a 10 min treatment with the 2.25 mg TiO_2/Au/Mg motors (green, f), as compared with different control experiments (a−e). Control experiments (for the two compounds) include operation (a) without any treatment in the dark, (b) moving TiO_2/Au/Mg motors in the dark, (c) moving Al_2O_3/Au/Mg micromotors (with passive surface) under UV light, (d) UV light only without micromotors, (e) static TiO_2/Au/Mg micromotor in UV light, and (f) moving TiO_2/Au/Mg motors under UV light. Other conditions (A−D) include total volume of the contaminated solution (containing 0.08 M NaCl and 0.075% Triton X-100), 600 μL. Experiments performed at room temperature.

A series of control experiments, displayed in Figure 4C, were carried out to elucidate the effect and role of the different components and processes involved in the enhanced photocatalytic activity of the self-propelled water-powered micromotors. For example, Figure 4C evaluates the removal of MP under various conditions (a−f). A dramatic decrease of absorbance signal, corresponding to 95% degradation, is observed following treatment with the moving TiO_2/Au/Mg micromotors under UV light irradiation (green line, f). In contrast, only a negligible removal (<12%) of this organophosphorus compound is observed in the different control experiments, involving (a) no treatment in dark, (b) movement of TiO_2/Au/Mg motors in dark, (c) movement of Al_2O_3/Au/Mg micromotors (with passive surface) under UV light, (d) UV light alone (without micromotors), and (e) static TiO_2/Au/Mg micromotors under UV light. The comparison between the static TiO_2/Au/Mg micromotors under UV irradiation and UV irradiation alone (e *vs* d) indicates that the presence of the TiO_2 photoactive layer is crucial for the degradation process. However, compared to the static TiO_2/Au/Mg micromotors (without movement), the self-propelled micromotors display a ~7-fold faster degradation (e *vs* f). These data clearly indicate that the new self-propelled photocatalytic platform offers significantly faster and greatly improved destruction of MP. Evidently, the large-scale collective motion of the micromotors and the corresponding hydrogen bubbles promote efficient fluid transport and mixing and accelerate the decontamination process. The fast motion enables also efficient *in situ* self-cleaning of the TiO_2 surface, hence reducing the passivation effect of adsorbed species to further enhance and retain photocatalytic activity.[38] Overall, the water-driven motion of the photocatalytic layer improves both the yield and the speed of the decontamination process.

The versatility of the new photocatalytic micromotor method has been demonstrated by degradation of different CWA simulants. Particular attention has been given to bis(4-nitrophenyl)phosphate, an agent which is highly resistant toward hydrolytic cleavage.[39] As illustrated in Figure 4D, 95.7% of the b-NPP agent decomposed within 10 min using the self-propelled TiO_2/Au/Mg micromotors, as compared to only 15.2% using the same amount of TiO_2/Au/Mg micromotors but without motion. Additional experiments aimed toward the degradation of 4-nitrophenol (a hydrolysis product of MP and b-NPP; Supporting Information Figure S2) confirm that the decomposition process occurs primarily through redox reactions that promote

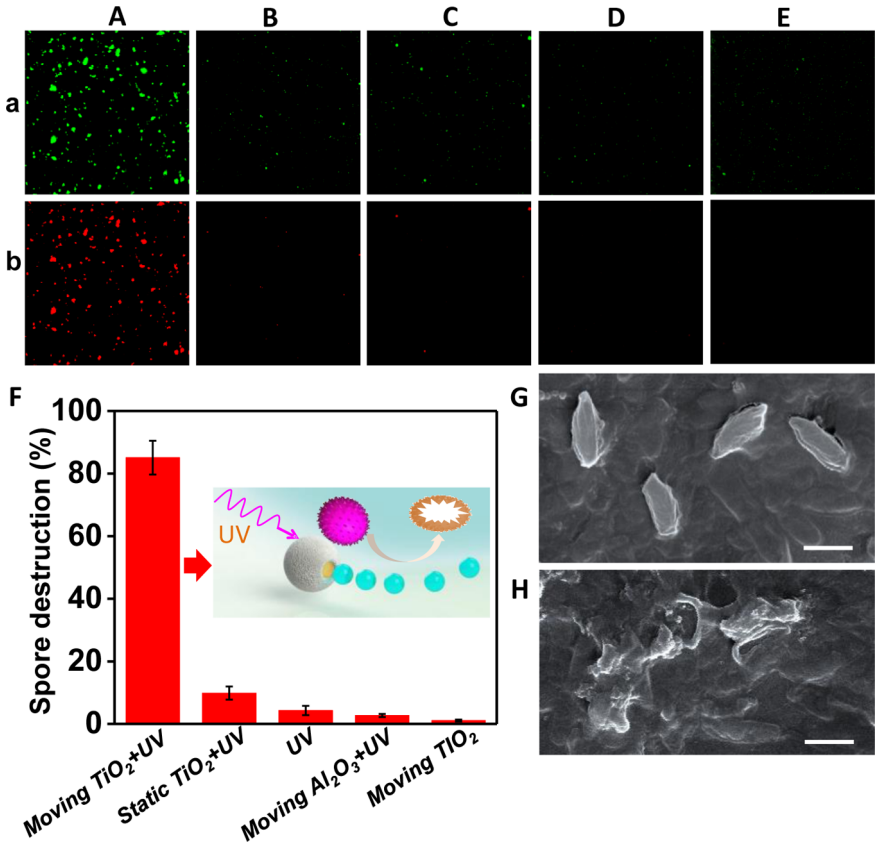

Figure 5. TiO_2/Au/Mg motor-driven photocatalytic degradation of BWA, along with different control experiments. Fluorescence images of (a) total Bacillus globigii spores in green and (b) destructed spores in red after 10 min treatment of (A) moving TiO_2/Au/Mg motors in UV light, (B) moving TiO_2/Au/Mg motors in the dark, (C) moving Al_2O_3/Au/Mg micromotors (with passive surface) in UV light, (D) UV light only, and (E) static TiO_2/Au/Mg micromotors under UV light. (F) Statistical plot showing the spore destruction efficiency by the different treatments. (G) SEM images of the intact spores and (H) ruptured spores following the light-driven treatment by the moving TiO_2/Au/Mg motors. Scale bar, 1 μm. Other conditions: total volume of the contaminated solution = 600 μL (containing 0.08 M NaCl and 0.075% Triton X-100), motor number = 3.08×10^5, bacteria concentration 2.57×10^{10} CFU/mL.

complete mineralization rather than hydrolysis. The complete mineralization of nerve agents and phenolic compounds is attributed to the redox reaction carried out by the highly active radicals and anions generated on the UV-irradiated TiO_2/Au surface.[6] The proposed mechanism for the photocatalytic degradation and reaction pathways of different pollutants is detailed in the Supporting Information (Figure S1 and Scheme S1). Compared to the recent use of peroxide-driven microrockets for pollutant degradation,[29,30] the present strategy leads to a complete and rapid oxidative degradation of persistent chemical pollutants to nonharmful mineralized products without the addition of external peroxide fuel and decontaminating reagents.

The new self-propelled photocatalytic platform also offers significant improvement in the degradation of biological warfare agents. The efficient antispore activity of the TiO_2/Au/Mg micromotors was demonstrated toward the inactivation of *Bacillus globigii* spores, a surrogate species of *Bacillus anthracis* spores. *Bacillus anthracis* is of particular concern among potential biological warfare agent since it is a highly pathogenic organism and can easily be produced in large numbers in the spore form. These experiments were performed by immersing 2.25 mg of TiO_2/Au/Mg motors (3.08×10^5 in number) in 600 μL of contaminated solution containing 2.57×10^{10} CFU/mL of the intact spore under UV irradiation, with the micromotors generating reactive oxidative species and imparting significant fluid transport during the decontamination processes. Such autonomous movement results in a substantial improvement in the efficiency of the TiO_2 photodegradation reactions (compared to the static TiO_2-coated microparticles). After the deactivation process, fluorescent imaging was used to evaluate the viability of the spores in the supernatant. Syto-9 dye (green) was used to label all the spores, both intact and ruptured ones, while propidium iodide dye (red) was used to label the ruptured spores. Figure 5A shows fluorescence image of (a) total *B. globigii* spores (in green) and (b) ruptured spores (in red) by using the moving TiO_2/Au/Mg motors under 10 min UV irradiation. Different control experiments were carried out using the same period, including (B) moving TiO_2/Au/Mg motors in the dark, (C) moving Al_2O_3/Au/Mg micromotors (containing passive surface) in UV light, (D) UV light only (without motors), and (E) static TiO_2/Au/Mg micromotors under

UV light. As illustrated in Figure 5B–E, negligible spore inactivation (ranging from 1.1 to 9.8%) is observed in all control experiments. In contrast, a significant (86%) damage of the spores was achieved with the moving TiO_2/Au/Mg motors following a 10 min UV irradiation, reflecting the efficient antispore activity of the photocatalytic micromotors (compared to the static TiO_2 microparticles). Note that while the intact spores are usually widely dispersed (Figure 5B–E), the destructed spores tend to aggregate together (Figure 5A).

To confirm the above observations and to gain further understanding of the spore destruction, we used SEM to examine the morphology of the treated and untreated spores. Figure 5 displays SEM images of *Bacillus globigii* spores before (G) and after (H) 10 min UV irradiation in the presence of the moving TiO_2/Au/Mg motors. These images clearly illustrate the dramatic change of the cell morphology and structure following the photocatalytic micromotor treatment. The spores are observed to coalesce and shrink; these morphological changes can be attributed to the surface and internal damage induced by the highly reactive oxygen species generated on the TiO_2 surface.[40,41] This efficient treatment thus breaks the cell membrane and converts the spore to the organic debris depicted in Figure 5H.

CONCLUSIONS

In conclusion, we have developed water-driven magnesium-based spherical micromotors coated with a highly photoactive titanium dioxide film (containing gold nanoparticles) for the efficient photocatalytic decomposition of biological and chemical warfare agents. The practical utility of the new micromotors has been demonstrated for the effective degradation of surrogate species of *Bacillus anthracis* spores and the hard-to-decompose bis(4-nitrophenyl)phosphate chemical warfare agent. Compared to the peroxide-driven micromotors, such decontaminating micromotors are self-propelled in natural water matrices in the presence of surfactant without adding any external fuel. The enhanced photocatalytic degradation activity is attributed to the continuous motion of the TiO_2/Au/Mg micromotors and corresponding solution mixing and cleaning of the catalyst surface. The present study thus supports that the motion of micro/nanoscale reactive remediation platforms and the corresponding fluid transport can notably improve photochemical decontamination processes. Coupled with the elimination of the peroxide fuel requirement, these new capabilities pave the way for using the new micromotors for a variety of defense and environmental applications.

METHODS

Synthesis of TiO_2/Au/Mg Micromotors. The TiO_2/Au/Mg micromotors were prepared using magnesium microparticles (catalog #FMW20, TangShan WeiHao Magnesium Powder Co.; 20 ± 5 μm) as the base particles. The Mg particles were dispersed initially onto glass slides and coated with Au nanoparticles using a Denton Discovery-18 sputter system. The deposition was performed at room temperature with a dc power of 200 W and an Ar pressure of 2.5 mTorr. In order to obtain a thin film of Au nanoparticles on the Mg surface, rotation speed was set at a fast 100 rpm, and the deposition time was only 3 s. Then uniform TiO_2 coating was applied to the microspheres by atomic layer deposition (Beneq TFS200) at 100 °C for 120 cycles. For the Al_2O_3/Au/Mg micromotors in control experiments, the Mg particles were similarly sputtered with Au nanoparticles. The Al_2O_3 layer was deposited subsequently by ALD (100 °C for 120 cycles).

TiO_2/Au/Mg Janus Micromotor Propulsion. The autonomous propulsion of the TiO_2/Au/Mg micromotors in aqueous solution was obtained by adding a solution containing 0.08 M NaCl and 0.075% Triton X-100 (Fisher Scientific, Fair Lawn, NJ) as surfactant. Movement of the TiO_2/Au/Mg micromotors in real-life environmental medium was carried out by adding a solution containing 50% seawater and 0.075% Triton X-100 (Fisher Scientific, Fair Lawn, NJ) as surfactant. Videos were captured by an inverted optical microscope (Nikon Instrument Inc. Ti-S/L100), coupled with 10× and 4× objectives and a Hamamatsu digital camera C11440, using the NIS Elements AR 3.2 software.

Photocatalytic Experiments. Experiments were performed by adding different amounts (1.25–2.25 mg, corresponding to 1.71×10^5 to 3.08×10^5 in number) of TiO_2/Au/Mg motors to 600 μL of the contaminated solution, with 0.08 M NaCl as propulsion medium containing 0.075% Triton X-100. A xenon light source LAXC-100 with a power density of 300 W was used to irradiate the sample. Additional control experiments of Al_2O_3/Au/Mg motors with passive surface were performed in a similar fashion. Control experiments of static TiO_2/Au/Mg motors were performed in the absence of NaCl and the surfactant.

Spectrophotometric Measurement. Absorbance measurements were performed with a UV–vis spectrophotometer (UV-2450, Shimadzu). For photocatalytic degradation experiments of bis-(4-nitrophenyl)phosphate (C_o = 1.7 μM), methyl paraoxon (C_o =1.7 μM), and 4-nitrophenol (C_o = 0.13 mM), a 600 μL aqueous solution of 0.08 M NaCl and 0.075% Triton X-100 was used. After the photochemical reaction, the reaction mixture of b-NPP and MP was subjected to 0.05 M NaOH solution to convert the remaining amount of b-NPP and MP to 4-NP (hydrolysis product of b-NPP and MP) for spectophotometric analysis. Then, the remaining concentration of each pollutant in solution was calculated by measuring the absorbance of 4-NP at 400 nm. Stock solutions (b-NPP, MP, and 4-NP) were prepared daily in double distilled water and subsequently diluted to the required concentration.

Spore Destruction Experiments. *B. globigii* spores (solid biomaterial with 3.52×10^{12} cell/g, from The U.S. Army-Dugway Proving Ground) were weighed and diluted in deionized water to get 2.57×10^{10} CFU/mL. A cleaning step was necessary to eliminate some silica added to the cells to increase flowability (for dispersion purposes) by centrifuging the spores at a low speed of 1000 rpm for 1 min and separating the supernatant (the spores) from the precipitate (the silica). Spores were centrifuged again at 14 000 rpm for 10 min to remove the supernatant. Then 2.25 mg of micromotors was added to the spore pellet along with NaCl and Triton X-100 to get 0.08 M and 0.075% final concentration, respectively, in 600 μL of total solution. The mixture was irradiated with UV for 10 min; the motors were precipitated at 1000 rpm for 1 min, and the supernatant (containing cells) was centrifuged again at 14 000 rpm for 10 min to isolate the pellet. The pellet was resuspended in 100 μL of a mix of Syto-9 dye solution and propidium iodide dye previously dissolved in water following

the specifications of the L13152 LIVE/DEAD BacLight bacterial viability kit provider. Eppendorfs were covered with aluminum foil and gently mixed for 15 min. Subsequently, they were centrifuged at 14 000 rpm for 10 min, and the pellet was resuspended in 100 μL of water for counting. Fluorescent images of 2 μL drops were taken, and the number of intact and damaged cells was estimated by using the program ImageJ.

Conflict of Interest: The authors declare no competing financial interest.

Acknowledgment. This project received support from the Defense Threat Reduction Agency-Joint Science and Technology Office for Chemical and Biological Defense (Grant No. HDTRA1-13-1-0002 and HDTRA1-14-1-0064) and from the UCSD Calit2 Strategic Research Opportunities (CSRO) program. W.G. is a HHMI International Student Research fellow. R.D. and B.J.-S. acknowledge support from the China Scholarship Council (CSC) and the People Programme (Marie Curie Actions) of the EU seventh Framework Programme (REA Grant PIOF-GA-2012-326476), respectively. Authors thank W. Scott Jonas from the U.S. Army-Dugway Proving Ground for providing the *B. golobigii* spores.

Supporting Information Available: Proposed photocatalytic degradation mechanism, results of photocatalytic degradation of 4-NP, and supporting movies. This material is available free of charge *via* the Internet at http://pubs.acs.org.

REFERENCES AND NOTES

1. Russell, A. J.; Berberich, J. A.; Drevon, G. F.; Koepsel, R. R. Biomaterials for Mediation of Chemical and Biological Warfare Agents. *Annu. Rev. Biomed. Eng.* **2003**, *5*, 1–27.
2. Holty, J. E.; Bravata, D. M.; Liu, H.; McDonald, K. M.; Olshen, R. A.; Owens, D. K. Systematic Review: A Century of Inhalational Anthrax Cases from 1900 to 2005. *Ann. Int. Med.* **2006**, *144*, 270–278.
3. Kim, K.; Tsay, G. O.; Atwood, A. D.; Churchill, G. D. Destruction and Detection of Chemical Warfare Agents. *Chem. Rev.* **2011**, *111*, 5345–5403.
4. Hoffmann, M. R.; Martin, S. T.; Choi, W.; Bahnemann, D. W. Environmental Applications of Semiconductor Photocatalysis. *Chem. Rev.* **1995**, *95*, 69–96.
5. Linsebigler, A. L.; Lu, G. Q.; Yates, J. T. Photocatalysis on TiO_2 Surfaces: Principles, Mechanisms, and Selected Results. *Chem. Rev.* **1995**, *95*, 735–758.
6. Fujishima, A.; Hashimoto, K.; Watanabe, T. *TiO_2 Photocatalysis: Fundamentals and Applications*; BKC, Inc.: Tokyo, 1999.
7. Kau, J.-H.; Sun, D.-S.; Huang, H.-H.; Wong, M.-S.; Lin, H.-C.; Chang, H.-H. Role of Visible Light-Activated Photocatalyst on the Reduction of Anthrax Spore-Induced Mortality in Mice. *PLoS One* **2009**, *4*, e4167.
8. Trubitsyn, D. A.; Vorontsov, A. V. Experimental Study of Dimethyl Methylphosphonate Decomposition over Anatase TiO_2. *J. Phys. Chem. B* **2005**, *109*, 21884–21892.
9. Paxton, W. F.; Kistler, K. C.; Olmeda, C. C.; Sen, A.; St. Angelo, S. K.; Cao, Y.; Mallouk, T. E.; Lammert, P. E.; Crespi, V. H. Catalytic Nanomotors: Autonomous Movement of Striped Nanorods. *J. Am. Chem. Soc.* **2004**, *126*, 13424–13431.
10. Ozin, G. A.; Manners, I.; Fournier-Bidoz, S.; Arsenault, A. Dream Nanomachines. *Adv. Mater.* **2005**, *17*, 3011–3018.
11. Mallouk, T. E.; Sen, A. Powering Nanorobots. *Sci. Am.* **2009**, *300*, 72–75.
12. Wang, J. *Nanomachines: Fundamentals and Applications*; Wiley-VCH: Weinheim, Germany, 2013.
13. Mei, Y.; Solovev, A. A.; Sanchez, S.; Schmidt, O. G. Rolled-up Nanotech on Polymers: From Basic Perception to Self-Propelled Catalytic Microengines. *Chem. Soc. Rev.* **2011**, *40*, 2109–2119.
14. Guix, M.; Mayorga-Martinez, C. C.; Merkoçi, A. Nano/Micromotors in (Bio)chemical Science Applications. *Chem. Rev.* **2014**, *114*, 6285–6322.
15. Li, J.; Zhang, J.; Gao, W.; Huang, G.; Di, Z.; Liu, R.; Wang, J.; Mei, Y. Dry-Released Nanotubes and Nanoengines by Particle-Assisted Rolling. *Adv. Mater.* **2013**, *25*, 3715–3721.
16. Ebbens, S. J.; Howse, J. R. In Pursuit of Propulsion at the Nanoscale. *Soft Matter* **2010**, *6*, 726–738.
17. Sanchez, S.; Pumera, M. Nanorobots: The Ultimate Wireless Self-Propelled Sensing and Actuating Devices. *Chem.—Asian J.* **2009**, *4*, 1402–1410.
18. Wang, J. Can Man-Made Nanomachines Compete with Nature Biomotors? *ACS Nano* **2009**, *3*, 4–9.
19. Solovev, A. A.; Mei, Y.; Bermudez Urena, E.; Huang, G.; Schmidt, O. G. Catalytic Microtubular Jet Engines Self-Propelled by Accumulated Gas Bubbles. *Small* **2009**, *5*, 1688–1692.
20. Huang, G.; Wang, J.; Mei, Y. Material Considerations and Locomotive Capability in Catalytic Tubular Microengines. *J. Mater. Chem.* **2012**, *22*, 6519–6525.
21. Wang, J.; Gao, W. Nano/Microscale Motors: Biomedical Opportunities and Challenges. *ACS Nano* **2012**, *6*, 5745–5751.
22. Solovev, A. A.; Xi, W.; Gracias, D. H.; Harazim, S. M.; Deneke, C.; Sanchez, S.; Schmidt, O. G. Self-Propelled Nanotools. *ACS Nano* **2012**, *6*, 1751–1756.
23. Campuzano, S.; Orozco, J.; Kagan, D.; Guix, M.; Gao, W.; Sattayasamitsathit, S.; Claussen, J. C.; Merkoci, A.; Wang, J. Bacterial Isolation by Lectin-Modified Microengines. *Nano Lett.* **2012**, *12*, 396–401.
24. Gao, W.; Wang, J. Synthetic Micro/Nanomotors in Drug Delivery. *Nanoscale* **2014**, *6*, 10486–10494.
25. Balasubramanian, S.; Kagan, D.; Hu, C.-M.; Campuzano, S.; Lobo-Castañon, M. J.; Lim, N.; Kang, D. Y.; Zimmerman, M.; Zhang, L.; Wang, J. Micromachine-Enabled Capture and Isolation of Cancer Cells in Complex Media. *Angew. Chem., Int. Ed.* **2011**, *50*, 4161–4164.
26. Xi, W.; Solovev, A. A.; Ananth, A. N.; Gracias, D. H.; Sanchez, S.; Schmidt, O. G. Rolled-up Magnetic Microdrillers: Towards Remotely Controlled Minimally Invasive Surgery. *Nanoscale* **2013**, *5*, 1294–1297.
27. Nelson, B. J.; Kaliakatsos, I. K.; Abbott, J. J. Microrobots for Minimally Invasive Medicine. *Annu. Rev. Biomed. Eng.* **2010**, *12*, 55–85.
28. Gao, W.; Wang, J. The Environmental Impact of Micro/Nanomachines: A Review. *ACS Nano* **2014**, *8*, 3170–3180.
29. Soler, L.; Magdanz, V.; Fomin, V. M.; Sanchez, S.; Schmidt, O. G. Self-Propelled Micromotors for Cleaning Polluted Water. *ACS Nano* **2013**, *7*, 9611–9620.
30. Orozco, J.; Cheng, G.; Vilela, D.; Sattayasamitsathit, S.; Vazquez-Duhalt, R.; Valdés-Ramírez, G.; Pak, O. S.; Escarpa, A.; Kan, C.; Wang, J. Micromotor-Based High-Yielding Fast Oxidative Detoxification of Chemical Threats. *Angew. Chem., Int. Ed.* **2013**, *52*, 13276–13279.
31. Soler, L.; Sanchez, S. Catalytic nanomotors for Environmental Monitoring and Water Remediation. *Nanoscale* **2014**, *6*, 7175–7182.
32. Guix, M.; Orozco, J.; Garcia, M.; Gao, W.; Sattayasamitsathit, S.; Merkoci, A.; Escarpa, A.; Wang, J. Superhydrophobic Alkanethiol-Coated Microsubmarines for Effective Removal of Oil. *ACS Nano* **2012**, *6*, 4445–4451.
33. Moo, J. G. S.; Wang, H.; Zhao, G.; Pumera, M. Biomimetic Artificial Inorganic Enzyme-Free Self-Propelled Microfish Robot for Selective Detection of Pb^{2+} in Water. *Chem.—Eur. J.* **2014**, *20*, 4292–4296.
34. Gao, W.; Feng, X.; Pei, A.; Gu, Y.; Li, J.; Wang, J. Seawater-Driven Magnesium Based Janus Micromotors for Environmental Remediation. *Nanoscale* **2013**, *5*, 4696–4700.
35. Mou, F.; Chen, C.; Ma, H.; Yin, Y.; Wu, Q.; Guan, J. Self-Propelled Micromotors Driven by the Magnesium−Water Reaction and Their Hemolytic Properties. *Angew. Chem., Int. Ed.* **2013**, *52*, 7208–7212.
36. Su, R.; Tiruvalam, R.; He, Q.; Dimitratos, N.; Kesavan, L.; Hammond, H.; Lopez-Sanchez, J. A.; Bechstein, R.; Kiely, C. J.; Hutchings, G. J.; *et al.* Promotion of Phenol Photodecomposition over TiO_2 Using Au, Pd, and Au−Pd Nanoparticles. *ACS Nano* **2012**, *6*, 6284–6292.
37. Li, J.; Huang, G.; Ye, M.; Li, M.; Liu, R.; Mei, Y. Dynamics of Catalytic Tubular Microjet Engines: Dependence on Geometry and Chemical Environment. *Nanoscale* **2011**, *12*, 5083–5089.

38. Gogate, P. R.; Pandit, A. B. A Review of Imperative Technologies for Wastewater Treatment II: Hybrid Methods. *Adv. Environ. Res.* **2004**, *8*, 553–597.
39. Mancina, F.; Tecillab, P. Zinc(II) Complexes as Hydrolytic Catalysts of Phosphate Diester Cleavage: From Model Substrates to Nucleic Acids. *New J. Chem.* **2007**, *31*, 800–817.
40. Prasad, G. K.; Ramacharyulu, P. V. R. K.; Merwyn, S.; Agarwal, G. S.; Srivastava, A. R.; Singh, B.; Rai, G. P.; Vijayaraghavan, R. Photocatalytic Inactivation of Spores of *Bacillus anthracis* Using Titania Nanomaterials. *J. Hazard. Mater.* **2008**, *185*, 977–982.
41. Liou, J.-W.; Gu, M.-H.; Chen, Y.-K.; Chen, Y.-C.; Tseng, Y.-H.; Hung, Y.-J.; Chang, H.-H. Visible Light Responsive Photocatalyst Induces Progressive and Apical-Terminus Preferential Damages on *Escherichia coli* Surfaces. *PLoS One* **2011**, *6*, e19982.